Journal of Materials Chemistry B

Accepted Manuscript

ROYAL SOCIETY OF CHEMISTRY

www.rsc.org/materialsB

Active-targeted pH-responsive albumin–photosensitizer conjugate nanoparticles as theranostic agent

Gantumur Battogtokh, Young Tag Ko*

College of Pharmacy, Gachon University, Incheon 406-799, South Korea

*Corresponding author:

College of Pharmacy, Gachon University,

191 Hambakmoe-ro, Yeonsu-gu, Incheon 406-799, South Korea

Tel.: 82-32-899-6417; Fax: 82-32-820-4829

E-mail address: youngtakko@gachon.ac.kr

Abstract

The objective of this study was to develop an active-targeted, pH-responsive albumin–photosensitizer conjugate as a theranostic agent. Herein, a porphyrin derivative photosensitizer, pheophorbide-a (PheoA), was conjugated to bovine serum albumin (BSA) via a *cis*-aconityl linkage, and the conjugate was then linked with polyethylene glycosylated folate to improve targeting ability. Further, BSA-c-PheoA and folate (FA)-BSA-c-PheoA at a ratio of 2:1 self-assembled to form nanoparticles with a mean hydrodynamic diameter of 121.47 ± 11.60 nm. The release study exhibited that the photosensitizer was released 4.5-fold faster at pH 5.0 than at pH 7.4 when incubated for 24 h. Cellular uptake results showed that the FA-BSA-c-PheoA nanoparticles were readily taken up by B16F10 and MCF7 cancer cells. *In vitro* phototoxicity results showed that FA-BSA-c-PheoA NPs has higher efficacy on cancer cells compared to simple BSA-c-PheoA NPs. *In vivo* bioimaging results exhibited that that FA-BSA-c-PheoA NPs greatly accumulated into the tumor area as compared to free PheoA. These results show that our prepared FA-BSA-c-PheoA NP has the potential to be applied as a theranostic agent in photodynamic therapy and photodiagnosis of cancer.

Keywords: photosensitizer, albumin, self-assembled nanoparticle, *cis*-aconityl linkage, pheophorbide-a.

1. Introduction

Over the past few decades, photodynamic therapy (PDT), which is a combination of a photosensitizer (PS), light, and molecular oxygen, against invasive disorders, e.g., cancer, has received increased attention from researchers and physicians because the therapy is more selective than other widely used therapies, such as chemotherapy and radiotherapy [1]. In addition, most PSs can be employed as imaging agents for photodiagnosis because they emit strong fluorescence upon light treatment [2]. However, PDT is still not widely applied clinically owing to the drawbacks of PSs, including poor water solubility, low selectivity for the target area, and prolonged skin phototoxicity [3]. In order to overcome these weaknesses of PSs, many studies regarding PS delivery have been performed using carrier systems, such as encapsulation in liposomes [4], incorporation into micelles [5], and conjugation to biopolymers [6, 7]. Nevertheless, to date, none of these have been approved by the US Food and Drug Administration (FDA).

Nanomaterials provide attractive drug vehicles for cancer treatment because of their specific tumor features, including their leaky vasculature and defective lymphatic drainage systems, which allow nanoparticles (NPs) to accumulate in tumor tissue through the enhanced permeability and retention effect [8-10].

Albumin-based nanocarrier systems represent an attractive strategy, since albumin is a component of blood and is highly stable in the blood stream with different drug binding sites within the molecule [11]. Moreover, albumin accumulates in malignant and inflamed tissues through the enhanced permeability and retention effect [12, 13]. Recently, many studies regarding albumin-related carrier systems for drug molecules have been published, such as a nanoparticulate composite of human serum albumin and paclitaxel [14], peptide–albumin

conjugation to efficiently deliver therapeutic peptides [13], and PS–albumin conjugates [15]. Among them, a paclitaxel-loaded albumin nanoaggregate (Abraxane®) was approved by the US FDA for the treatment of various cancers [16, 17]. These achievements prove that albumin is a promising carrier for drug delivery.

The challenge of improving the imaging and therapeutic properties of photosensitizers for photodiagnosis and PDT could be achieved through the preparation of active-targeted nanoformulations activated upon exposure to stimuli (e.g., low pH and enzymes) at the target site. So far, several studies on PS delivery have focused on PS–macromolecule conjugates with and without stimuli-cleavable linkage, or PS-loaded NPs [18-21]. However, to the best of our knowledge, an active-targeted albumin–PS conjugate with a pH-responsive linkage has not yet been published elsewhere.

In this study, we proposed to synthesize a folate-targeted albumin–PS conjugate with a stimuli-responsive linkage (*cis*-aconityl) and prepare self-assembling NPs by using the conjugate. In this way, the PS could be selectively delivered to tumor cells overexpressing folate receptors by endocytosis and then released from the endosomes or lysosomes by cleavage of the linkage at low pH. An advantage of direct conjugation of the PS to the carrier system (albumin) is that the PS could be delivered into the target site in the conjugated form, rather than being physically entrapped within NPs, which may release their payload before reaching the target site [22]. Furthermore, grafting folate to the bovine serum albumin-*cis*-aconityl-PS (BSA-c-PS) molecule increases the specificity of the targeting, resulting in the ability to identify folate-receptor expressing tumors because the PS has a strong fluorescence emission at around 670 nm.

2. Materials and Methods

2.1. Reagents

BSA, folic acid, and *cis*-aconitic anhydride were obtained from Sigma-Aldrich (St. Louis, Missouri), and pheophorbide-a (PheoA) was purchased from Frontier Scientific, Ltd. (Logan, UT). All other reagents were purchased from Sigma-Aldrich or Tokyo Chemical Industry (Tokyo, Japan), unless otherwise stated.

2.2. Synthesis of the *cis*-acotinyl–PheoA conjugate

PheoA-ethylenediamine (PheoA-EDA) was prepared according to the previous methodology [23]. The prepared PheoA-EDA (100 mg, 0.16 mmol) was then dissolved in 5 mL of a mixture of methanol and dichloromethane (DCM), and to this solution, *cis*-aconitic-anhydride (122.9 mg, 0.787 mmol) in 1,4-dioxane (1 mL) was slowly added at 0 °C under argon gas and in dark. The reaction mixture was stirred for 2 h at room temperature (RT), and the reaction progress was monitored by thin-layer chromatography (TLC) with DCM and methanol (98:2) as the eluent. After the reaction was completed, the residue was crystallized from a mixture of methanol and DCM and diethyl ether and washed twice with ether. Finally, the solid was dried under vacuum and analyzed by proton nuclear magnetic resonance (^{1}H NMR) spectroscopy (600 MHz, Bruker Billerica, MA) as well as Fourier transform infrared (FT-IR) spectroscopy (Bruker, Billerica, MA) and UV-vis spectroscopy (Cary 60, Agilent Technology, Santa Clara, CA).

2.3. Synthesis of BSA-c-PheoA conjugate

Cis-aconityl PheoA (c-PheoA; 30 mg, 0.047 mmol) in 5 mL of chloroform was reacted with *N*-hydroxysuccinimide (NHS; 5.4 mg, 0.047 mmol) and ethylene-carbodiimide (14.6 mg, 0.094 mmol) in the presence of five drops of triethylamine for 6 h at RT. The reaction progress was

monitored by TLC on a silica gel plate with methanol/DCM (1:5) as the eluent. After purifying on a silica gel column, the aliquot was dried under vacuum, resulting powder in scented c-PheoA-EDA.

Subsequently, BSA (126 mg, 0.0019 mmol) was dissolved in 2 mL of phosphate-buffered saline (PBS; pH adjusted to 8.5 by adding 0.1 M sodium bicarbonate). To this solution, succinated c-PheoA-EDA in 0.2 mL of DMSO was slowly added and stirred for 1 h at RT. The reaction product was passed through a Sephadex G25 column (DP-10; GE Healthcare, Little Chalfont, UK) to remove impurities and then freeze-dried for 48 h by lyophilizer. The conjugation was confirmed by UV-vis and FT-IR spectroscopy. The PheoA content was determined by UV-Vis spectroscopy.

2.4. Synthesis of FA-PEG-BSA-c-PheoA conjugate

Initially, polyethylene glycosylated (PEGylated) FA was prepared by slightly modifying previous methods [24, 25]. Briefly, 100 mg (0.225 mmol) of FA were dissolved in 1 mL of dry dimethyl sulfoxide (DMSO) and added to 25.9 mg (0.225 mmol) of NHS and 92.5 mg (0.45 mmol) of dicyclohexyl carbodiimide (DCC) in the presence of three drops of triethylamine. After stirring for 3 h at RT, 281 mg (0.14 mmol) of PEG2000–amine (1:1.6 molar ratio of NH_2–PEG/folate) were added into the activated FA, followed by stirring for 2 h at RT under nitrogen. The organic solvent was removed by rotary evaporator, and the remainder was rehydrated with 6 mL of deionized water and then centrifuged at 4000 rpm for 10 min to remove insoluble byproducts. Subsequently, the supernatant was lyophilized for 48 h. The obtained product was analyzed by ^{1}H NMR and FT-IR spectroscopy.

Further, FA-PEG-OH (12.5 mg, 0.0052 mmol) in 2 mL of anhydrous tetrahydrofuran (THF)

was reacted with 6.56 mg (0.025 mmol) of *N,N*-disuccinimidyl carbonate in 2 mL of THF in the presence of 2 mg (0.016 mmol) of 4-(dimethylamino) pyridine in 2 mL of THF for 3 h at RT under argon to activate the hydroxyl group. The reaction progress was monitored using TLC with DCM and ethyl acetate (98:2) as the eluent. After the reaction was completed, the mixture was evaporated under vacuum. The resulting succinated FA-PEG in 0.4 mL of DMSO was added to 60 mg (0.00086 mmol) of BSA pre-dissolved in 5 mL of 0.1 M sodium bicarbonate (pH 8.3) at a rate of 200 µL per 5 min and stirred for 1.5 h under argon. The reaction product was passed through a Sephadex G25 column to remove impurities and freeze-dried for 48 h by lyophilizer. The conjugation was confirmed by UV-vis and FT-IR spectroscopy.

2.5. Preparation of folate-targeted BSA-c-PheoA NPs

Folate-targeted BSA-c-PheoA NPs were prepared by simply mixing under sonication. Briefly, BSA-c-PheoA (10 mg) and FA-BSA-PheoA (5 mg) at a weight ratio of 2:1 were dissolved in 4 mL of PBS. This mixture was stirred for 15 min at RT. The resulting solution was sonicated at 4 °C for 30 min using a bath-type sonicator (Branson, Danbury, Connecticut). To remove aggregates, the NP solution was centrifuged at 2000 rpm for 3 min. The NP hydrodynamic diameter and zeta potential were measured by dynamic light scattering and electrophoretic light scattering (laser Doppler) using a zeta-potential and particle size analyzer (ELSZ-1000, Otsuka Electronics Co, Osaka, Japan). Scattered light was detected at 23 °C at an angle of 90°. A viscosity of 0.933 mPa and a refractive index of 1.333 were used for data analysis. The morphology of the nanostructure was also observed by transmission electron microscopy (TEM). Nanostructured formulations were stained with 2% uranyl acetate and destained with double-

distilled water. They were then placed on copper grids with films, dried for 10 min, and observed using TEM (JEM 1010, JEOL, Tokyo, Japan).

The fluorescence emission spectra were measured by a Cary Eclipse fluorescence spectrophotometer (Agilent Technology, Santa Clara, CA). The UV-vis absorption spectra were acquired by a Cary 60 UV-vis spectrophotometer (Agilent Technology, Santa Clara, CA). All optical measurements were performed at RT.

2.6. Detection of singlet oxygen

To detect the singlet oxygen generation (SOG) of FA-BSA-c-PheoA, 9, 10 – dimethylanthracene (DMA) was used [26]. To the FA-BSA-c-PheoA (1.5 μ/mL PheoA) in DW was added DMA (20 mM) in dimethylformamide with the final concentration 20 μM. Then the solutions were irradiated with a 670 nm laser. DMA fluorescence emission was measured with Cary Eclipse fluorescence spectrophotometer (Agilent Technology, Santa Clara, CA) under 360 nm excitation. The sample's SOG was evaluated by the DMA fluorescence decrease compared with the background.

2.7. *In vitro* pH-sensitive drug release study

In vitro drug release was investigated using previously reported methods with minor modifications [27, 28]. An FA-BSA-c-PheoA NP solution (200 μL, 50 μg/mL of PheoA) was prepared and added to a Mini-Pur-A-Lyzer tube with a molecular weight cut-off of 12 kDa (Sigma-Aldrich). The tubes were immersed in 3 mL of PBS (pH 7.4) containing 0.5% (w/v) Tween 80 and incubated at 37 °C whilst rotating at 50 rpm. The entire volume of dissolution medium (3 mL) was collected at various time points (1, 2, 3, 4, 6, 9, 24, and 48 h) and replaced with 3 mL of fresh medium at 37 °C. The amounts of PheoA released were assessed by

measuring the fluorescence emission at ex. 405 and em. 675 nm using an Synergy MX fluorometer (Biotek, Winooski, VT)

2.8. Study of *in vitro* cellular uptake and targeting by confocal microscope

The murine melanoma cell line B16F10 and human breast adenocarcinoma cell line MCF-7 were seeded onto 6-well plates at 6×10^5 cells/well in 2 mL of Dulbecco's Modified Eagle's Medium supplemented with 10% fetal bovine serum 24 h before experimentation. The PheoA, BSA-c-PheoA, FA-BSA-c-PheoA, and FA-BSA-c-PheoA NPs (10 μg/mL of Pheo-A) were added to each well and incubated with the cells for 1.5 and 3 h at 37 °C. To visualize cell internalization, the cells were treated with 15 μL of 0.5 μM Lysotracker Green DND-26 (Life Technology, Eugene, Oregon) for 30 min and washed twice with cold PBS, fixed with 4% paraformaldehyde (2 mL) for 5 min, then washed twice with cold PBS. In the folate receptor blocking experiment, before treating with the FA-BSA-c-PheoA NPs, free FA (1 mM) was added, and the cells were incubated for 30 min. Afterwards, the slides were rinsed once with PBS. Finally, the slides were mounted with Fluoromount (Sigma, St. Louis, Missouri) and observed with an ECLIPSE Ti confocal microscope (Nikon Instruments Inc., Melville, NY). The images were captured under a Lysotracker filter (green excitation 488/22 nm; emission 460/50 nm) and a QDot 655 filter (red excitation 410/40 nm; emission 675/50 nm).

2.9. *In vitro* phototoxicity

The phototoxicity of the NPs was evaluated using a 3-(4,5-dimethylthiazol-2- yl)-2,5-diphenyltetrazolium bromide (MTT) assay after the light treatment. B16F10 cells or MCF7 cells were seeded onto a 96-well tissue culture plate (1.0×10^4 cells/well). After incubation at different concentrations of free PheoA, BSA-c-PheoA, FA-BSA-c-PheoA, or FA-BSA-c-Pheo

NP (0.375, 0.75, 1.5 and 3 μg/mL of PheoA) for **6** h, the cells were irradiated at a light intensity of 1.5 J/cm^2 using a 671 ± 1 nm LED laser source (Shanghai Dream Lasers Technology Co., Ltd, China) for 20 min. The dark toxicity of NPs and free PheoA without light treatment were also investigated. The cells were further incubated for 24 h, and the cell viability was evaluated by MTT assay. For the MTT assay, 10 μL of 5 mg/mL MTT solution was added to each cell-culture well and cultured for 4 h. Next 100 μL of dimethylsulfoxide was added to the culture, shaken for 10 s, and the absorbance was measured with an Epoch microplate spectrophotometer at 570 nm. Each group consisted of three wells; the means of their values were used as the measured values.

2.10. *In vivo* bio-imaging study

Animal experiments were performed according to protocols approved by the Institutional Animal Care and Use Committee at Gachon University. Athymic nude (Balb/c) mice were obtained from Orient-Bio (Seongnam, South Korea). The MCF7 tumor models were generated by subcutaneous injection of 1×10^6 cells in l00 μl PBS in to the right fat pat of nude mice. The mice were used for imaging when the tumor volume reached 100 mm^3. *In vivo* fluorescence imaging of PheoA in NPs, mice bearing MCF7 xenografted tumors were intravenously injected with free PheoA or FA-BSA-c-PheoA NPs (200 μl, 1 mg/kg for PheoA). Fluorescence imaging was performed with an IVIS optical imaging system (Caliper Life Sciences, Hopkinton, MA) at 1, 6, and 24 h post-injection. The PS spectrum was separated from autofluorescence by Living Image @3.1 software (Caliper Life Sciences).

To compare the tissue and tumor accumulation of free PheoA and FA-BSA-c-PheoA NPs, mice were sacrificed after 24 h following intravenous injection. The excised tissues included the livers, lungs, spleens, kidneys, skins, and hearts, as well as the tumors. Tissues were analyzed by

measuring the PheoA fluorescence intensity by using IVIS optical imaging system and a long wave emission filter (605 to 700 nm).

3. Results

3.1. Characterization of *cis*-aconityl-PheoA, BSA-c-PheoA, and FA-BSA-c-PheoA conjugates

All the synthesis schemes are illustrated in **Figure 1**. To obtain the BSA-c-PheoA conjugate, PheoA was first linked with tert-butyloxycarbonyl-protected ethylenediamine and PheoA-EDA was then prepared by removing the protecting group. The PheoA-EDA was conjugated with *cis*-aconitic anhydride, which is a pH-responsive cleavable linkage, through the reaction of a free amine group of PheoA-EDA with the anhydride group of *cis*-aconitic anhydride.

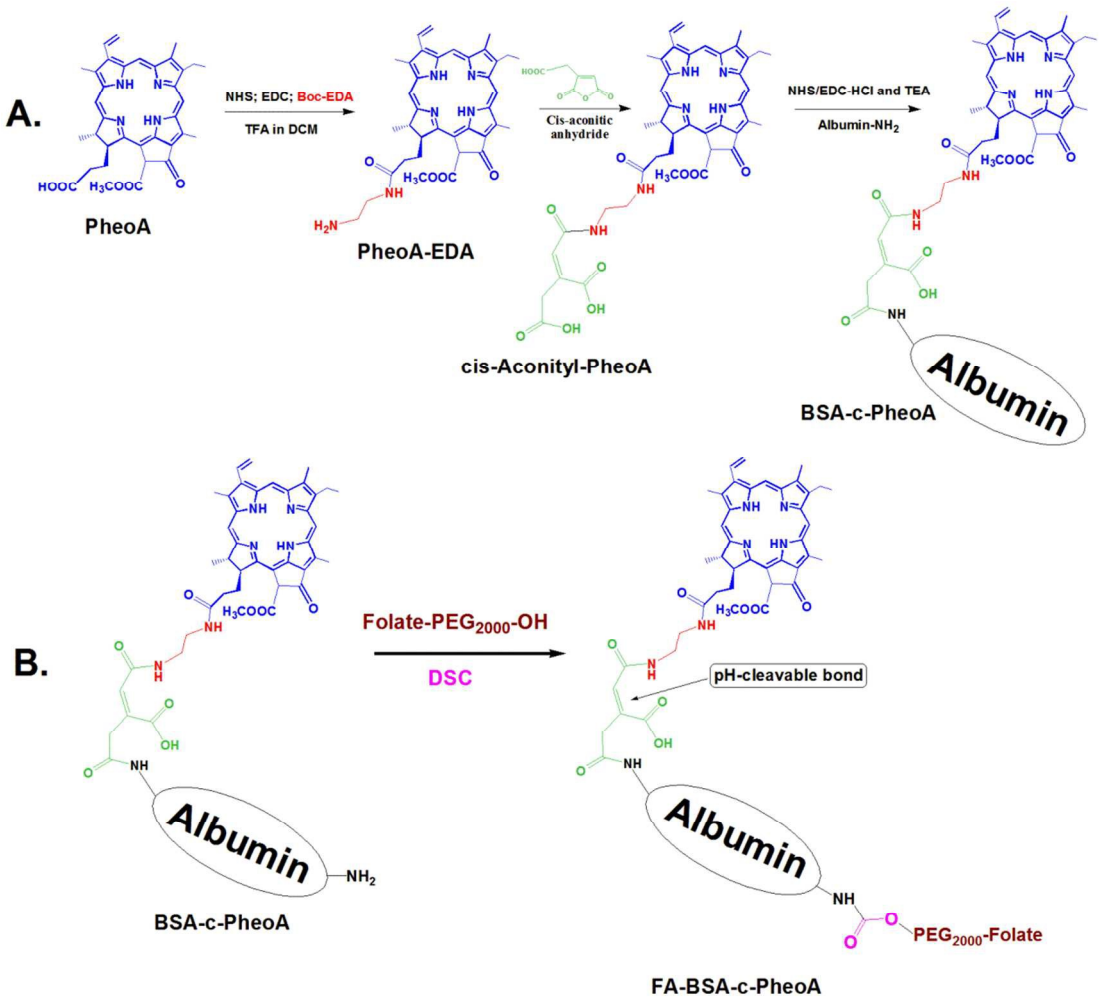

Figure 1. (A) Synthesis scheme for *cis*-aconityl pheophorbide-a (PheoA) and bovine serum albumin-*cis*-aconityl pheophorbide-a (BSA-c-PheoA). (B) Synthesis scheme for folate-targeted bovine serum albumin-cis-aconityl pheophobide-a (FA-BSA-c-PheoA). DCM: dichloromethane; EDC: 1-Ethyl-3-(3-dimethylaminopropyl)carbodiimide; NHS: N-hydroxysuccinimide; PEG: polyethylene glycol; TFA: trifluoroacetic acid; TEA: triethylamine.

The conjugates were analyzed by ^{1}H NMR and FT-IR spectroscopy. The formation of *cis*-aconityl PheoA was demonstrated by the appearance of significant signals at 7.7 ppm for the NH and 6.18–6.20 ppm for the CH=CH of the *cis*-aconityl linkage in addition to the major signals of

PheoA (at 9.8–8.9 ppm for methyl, 8.18 ppm for NH, 6.4 ppm for CH=CH, and 4.5–1.1 ppm for CH_3, CH, and CH_2 in the porphyrin backbone) in the proton NMR spectrum (**Figure S1A, B**).

Further, the obtained *cis*-aconityl PheoA (c-PheoA) was conjugated to BSA by the reaction between a carboxyl group of *cis*-aconityl-PheoA and an amine group of BSA in the presence of EDC/NHS activating reagents. The unreacted c-PheoA was removed by size exclusion chromatography. The amount of PheoA attached to BSA was determined to be five molecules per molecule of BSA from the UV-Vis calibration curve of PheoA at 675 nm (**Figure S2**). Furthermore, FT-IR spectroscopy (**Figure 2C**) also demonstrated the conjugation between BSA and c-PheoA with specific peaks at 3293.2, 1650.2, and 1538.8 cm^{-1} for the primary amine and amide (NH_2, C=O and N-H) of the albumin moiety and at 3495.7, 2959.4, 1735.8, 1376.4, and 1075.9 cm^{-1} for the N-H (stretching) in the pyrrole ring, the -CH- (stretching) in the ring, C=O (stretching), and C=C (stretching) pyrroles of *cis*-aconityl PheoA, respectively. To synthesize FA-BSA-c-PheoA, a folate-PEG-OH conjugate was prepared according to previous reports. The obtained folate-PEG-OH was attached to BSA-c-PheoA by using the coupling reagent *N,N*-disuccinimidyl carbonate. After purifying, there were determined to be 2.5 folate molecules per BSA-c-PheoA molecule by UV-Vis spectroscopy using the absorbance at 250 nm. The FT-IR spectrum (**Figure 2D**) showed that the intensity of the peaks at 1153.9, 1075.9, and 858.3 cm^{-1} in FA-BSA-c-PheoA corresponding to the ether (C-O-C) and aromatic C-H bending of FA-PEG, respectively, increased as compared with those in the spectrum of BSA-c-PheoA. In addition, a new peak at 949.2 cm^{-1} in the spectrum of FA-BSA-c-PheoA is assigned to the benzyl of the folate molecule.

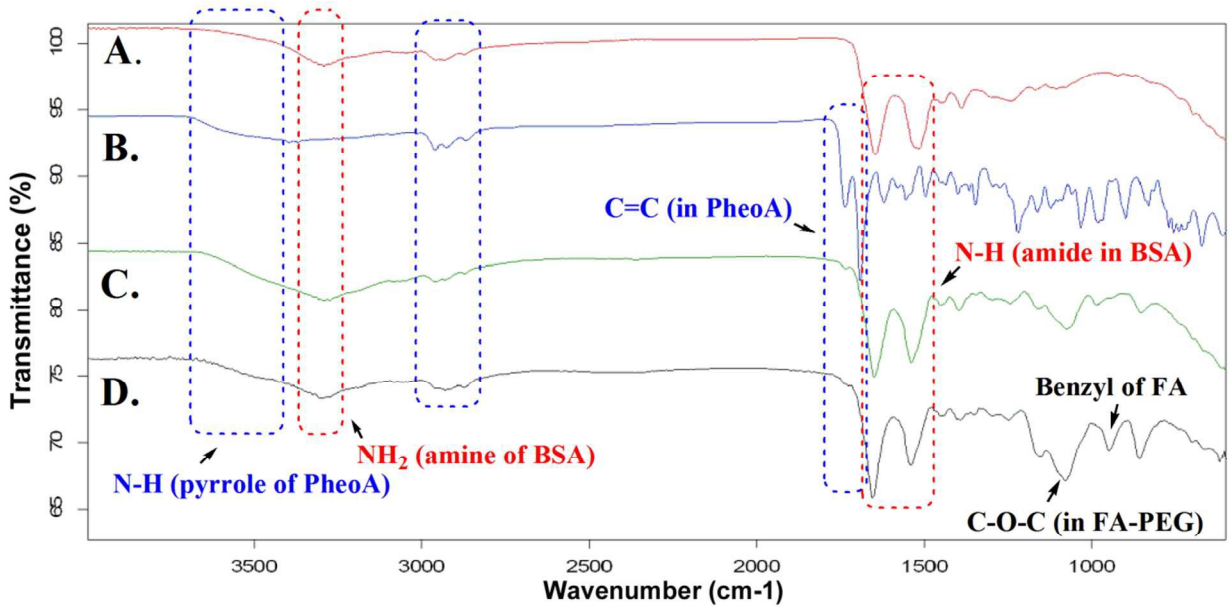

Figure 2. FT-IR spectra of bovine serum albumin (BSA) (A), pheophorbide-a (PheoA) (B), bovine serum albumin-*cis*-pheophorbide-a (BSA-c-PheoA) (C), and folate-bovine serum albumin-*cis*-pheophorbide-a (FA-BSA-c-PheoA) (D).

In addition, as illustrated in **Figure 3**, all conjugates were confirmed by UV-Vis spectroscopy through specific absorption peaks at 255 and 285 nm for folate and 275 nm for BSA (**black and blue lines**), the Soret band at 410 nm and the Q band at 670 nm for PheoA (**green line**), as well as a slight blue shift in the Soret band (from 410 nm to 390 nm) and a slight red shift in the Q band (from 670 nm to 675 nm) in the UV spectra of BSA-c-PheoA (**purple line**) and FA-BSA-PheoA (**red line**), respectively, likely due to the aqueos medium.

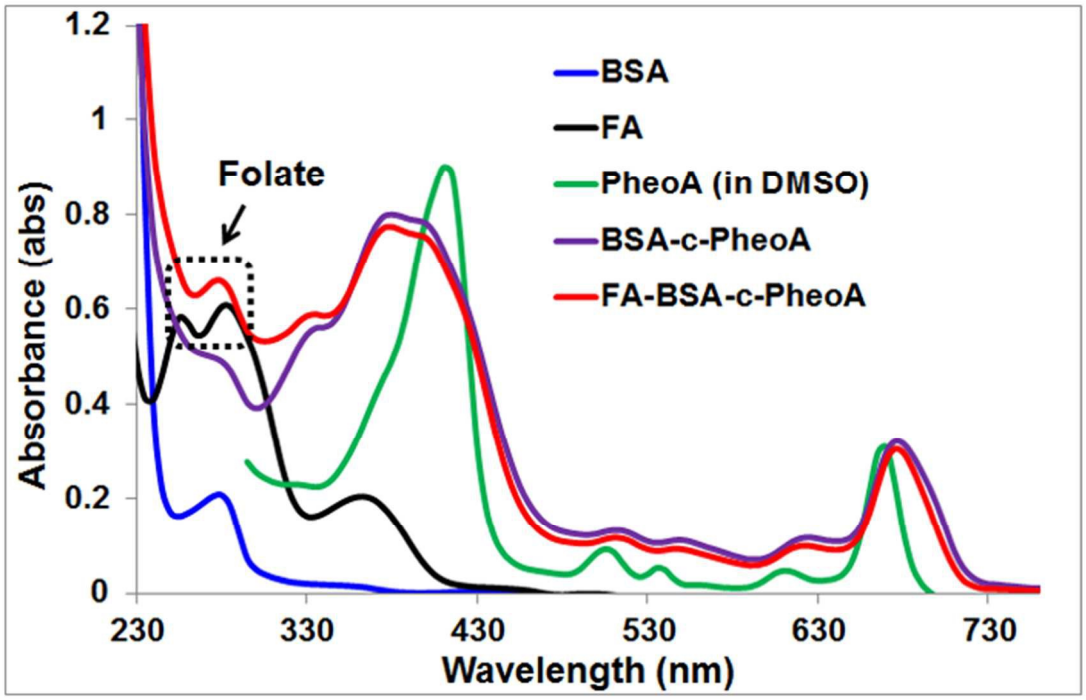

Figure 3. UV-vis absorption spectra: blue line for bovine serum albumin (BSA) in phosphate-buffered saline (PBS), black line for folate (FA) in dimethyl sulfoxide (DMSO), green line for pheophorbide-a (PheoA) in DMSO, purple line for bovine serum albumin-*cis*-pheophorbide-a (BSA-c-PheoA) in PBS, and red line for FA-BSA-c-PheoA in PBS.

3.2. Physicochemical characteristics of FA-BSA-c-PheoA NPs

The scheme used for the preparation of the NPs is shown in **Figure 4**. FA-BSA-c-PheoA NP was prepared from BSA-c-PheoA and FA-BSA-c-PheoA at a weight ratio of 2:1 by sonication.

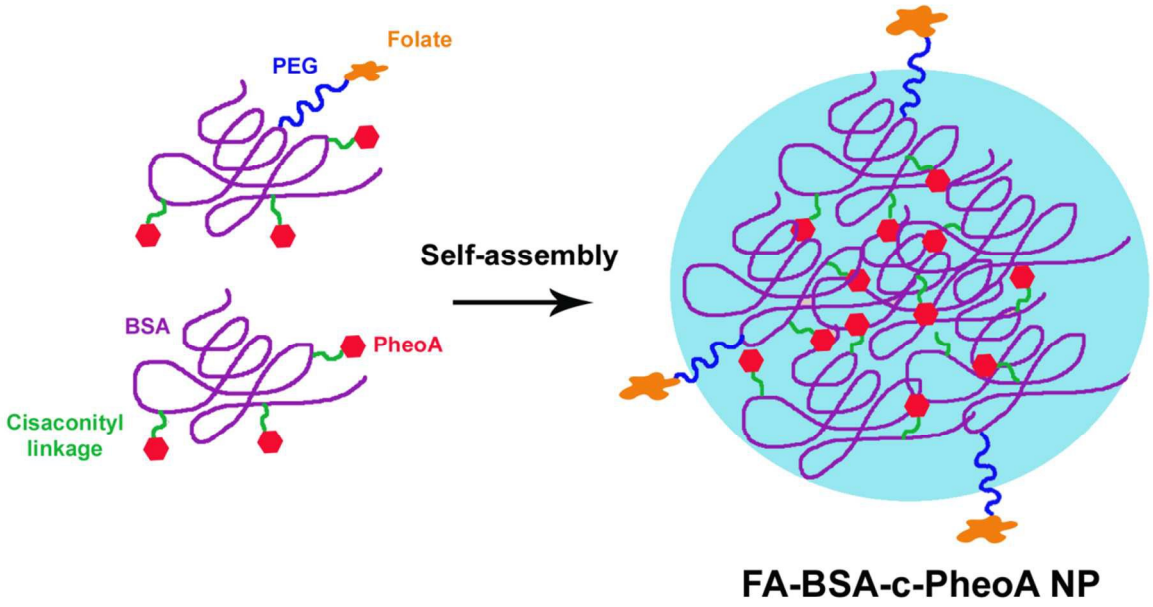

Figure 4. Scheme of the self-assembly of folate-bovine serum albumin-*cis*-aconityl pheophorbide-a NPs (FA-BSA-c-PheoA).

The size distribution (**Figure 5A**), polydispersity index, and zeta potential of the folate-BSA-c-PheoA NPs were found to be 121.47 ± 11.60 nm, 0.39 ± 0.01, and -31.6 ± 2.91 mV, respectively (**Table 1**), indicating that the NP could readily accumulate in tumors by the enhanced permeability and retention effect because of its optimal size (within the 200 nm size range). Size distribution of FA-BSA-c-PheoA NPs was slightly bigger than that of BSA-c-PheoA NPs, indicating that grafting of FA-PEG on surface increases the size.

Table 1. Physical characteristics of folate-bovine serum albumin-*cis*-aconityl pheophorbide-a (FA-BSA-c-PheoA) (mean ± S.D., n = 3).

Formulation	Size (nm)	Zeta Potential (mV)	PDI
BSA-c-PheoA NP	104.10 ± 9.35	-14.79 ± 1.63	0.49 ± 0.04
FA-BSA-c-PheoA NP	121.47 ± 11.60	-31.60 ± 2.91	0.39 ± 0.01

The TEM image (**Figure 5B**) shows that FA-BSA-c-PheoA is present as spherical NPs with a similar diameter to that obtained by dynamic light scattering. As shown in **Figure 5C**, the NPs in aqueous solution are clear, whereas free PheoA aggregated in aqueous solution.

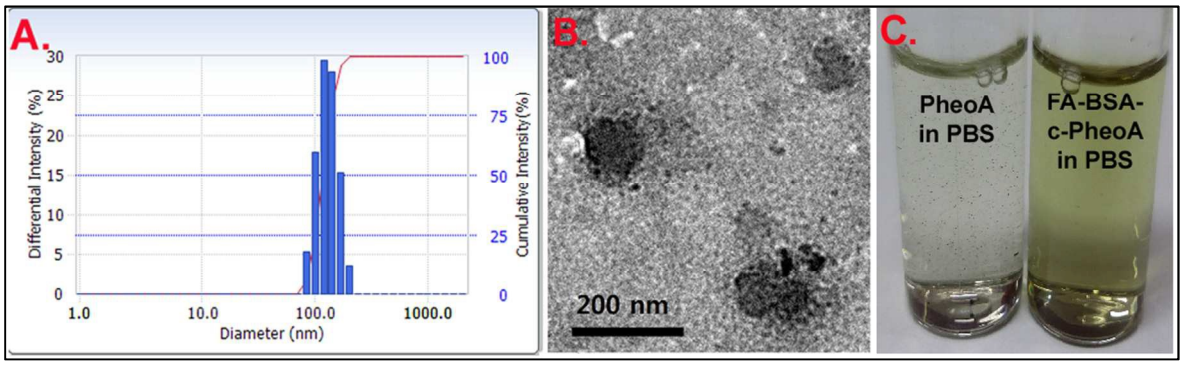

Figure 5. Nanoparticle characterization showing: (A) the size distribution and (B) the transmission electron microscopy image of the folate-bovine serum albumin-*cis*-aconityl pheophorbide-a nanoparticles (FA-BSA-c-PheoA NPs), and (C) the visibility of free PheoA and FA-BSA-c-PheoA in aqueous solution.

A comparison of the absorption and fluorescence spectra of free PheoA in PBS/DMSO, BSA-c-PheoA, FA-BSA-c-PheoA in PBS is shown in **Figure 6**. The same samples were used for both UV-vis absorbance and fluorescence analysis. The absorbance of the FA-BSA-c-PheoA NP was similar to that of free PheoA in PBS/DMSO, but the fluorescence was lower than that of free

PheoA, indicating that the fluorescence of the PS was quenched in the NPs. However, the fluorescence of the PS could be recovered through cleavage of the pH-responsive linkage in intracellular environment.

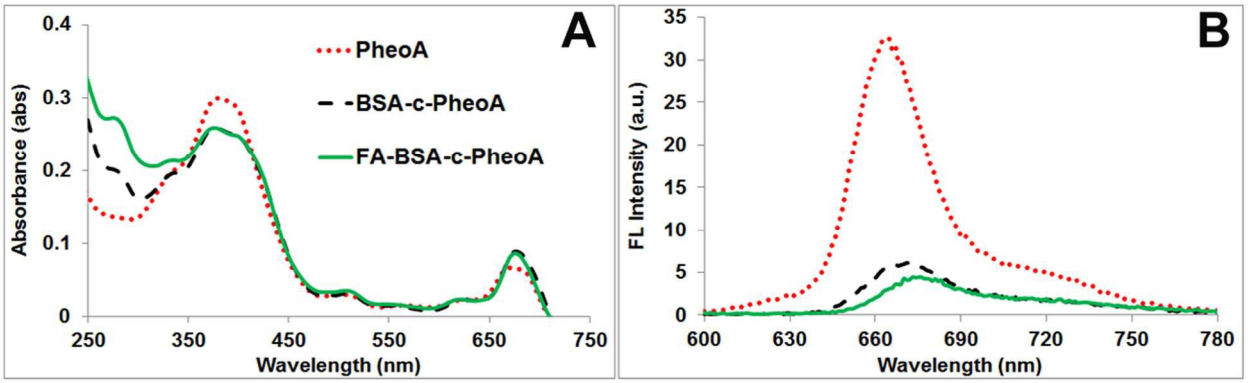

Figure 6. Comparison of the UV absorption (A) and fluorescence (B) spectra of free pheophorbide-a in PBS/dimethyl sulfoxide (DMSO), bovine serum albumin-*cis*-aconityl pheophorbide-a (BSA-c-PheoA) and folate bovine serum albumin-*cis*-aconityl pheophorbide-a (FA-BSA-c-PheoA) in PBS (equal concentration of PheoA at both case).

In order to claim the cleavage of *cis*-aconityl linkage, fluorescence measurement was performed time-dependently at different pH (5 and 7.4). The results (**Figure 7A**) showed that after 3 h incubation at pH 5, the fluorescence intensity increased 1.5-fold, indicating recovery of fluorescence of PheoA through the cleavage of *cis*-aconityl linkage; in contrast, the fluorescence intensity of PheoA at pH 7.4 was not affected much for 3 h incubation (**Figure 7B**).

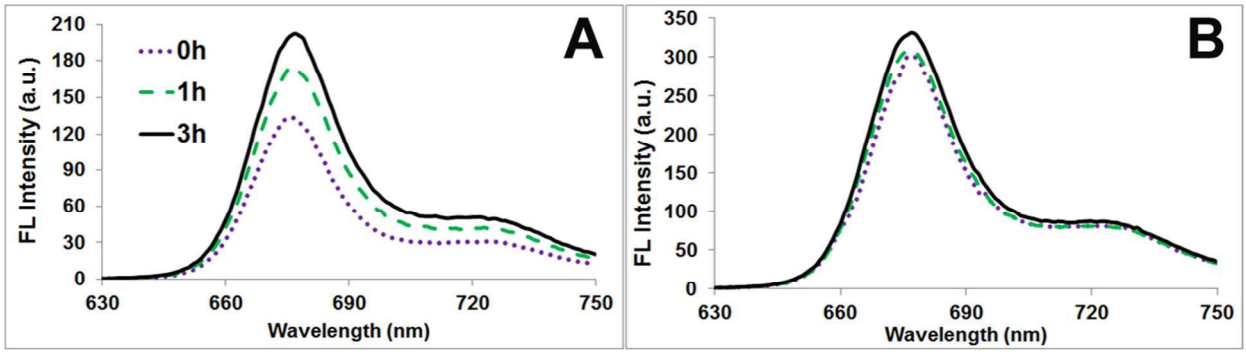

Figure 7. Recovery of fluorescence quenching through low pH: (A) fluorescence profile of FA-BSA-c-PheoA NP at pH 5.0 for 3h; (B) fluorescence profile of FA-BSA-c-PheoA NP at pH 7.4 for 3h.

The photodynamic effect of FA-BSA-c-PheoA was confirmed by measuring singlet oxygen using DMA as a detector [26, 29]. As shown in **Figures 8A** and **B**, the fluorescence intensity of DMA exhibits a time-dependent decrease, indicating singlet oxygen generated from FA-BSA-c-PheoA upon laser irradiation.

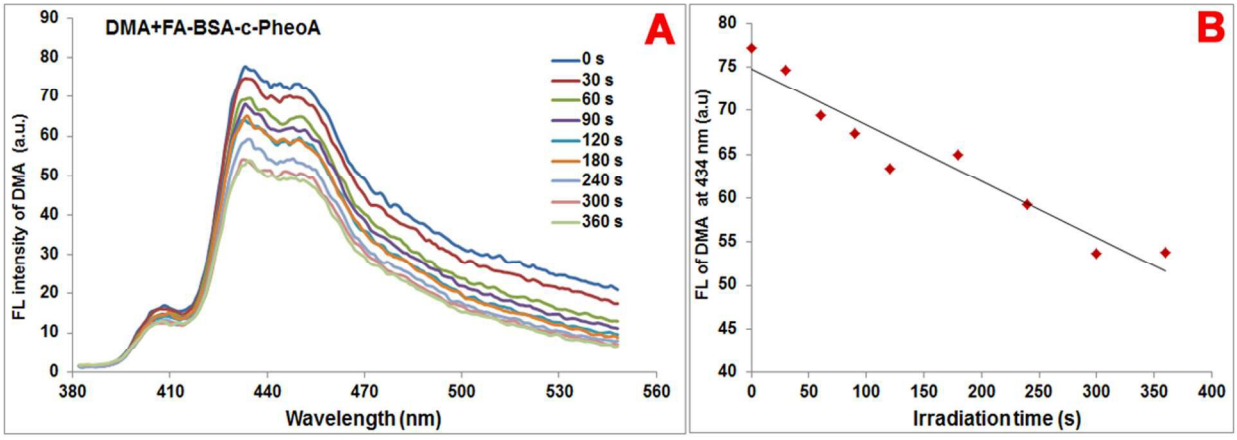

Figure 8. (A) Fluorescence emission spectra of FA-BSA-c-PheoA with DMA solution with the increase of laser irradiation time. (B) The fluorescence intensity change of DMA at 434 nm as a function of laser irradiation time.

Moreover, the release study (**Figure 9**) exhibited that the release of PheoA from FA-BSA-c-PheoA NPs was 4.5-fold greater at pH 5.0 than at pH 7.4 at 37 °C after incubation for 24 h, implying that the *cis*-aconityl linkage is cleaved at low pH, which is similar to an intracellular environment (endosomes or lysosomes). Concentration of released PheoA was determined based on the calibration curve as shown in **Figure S2**. **Figure 9B** shows that the size of the NP was effected though low pH, resulting in drug release.

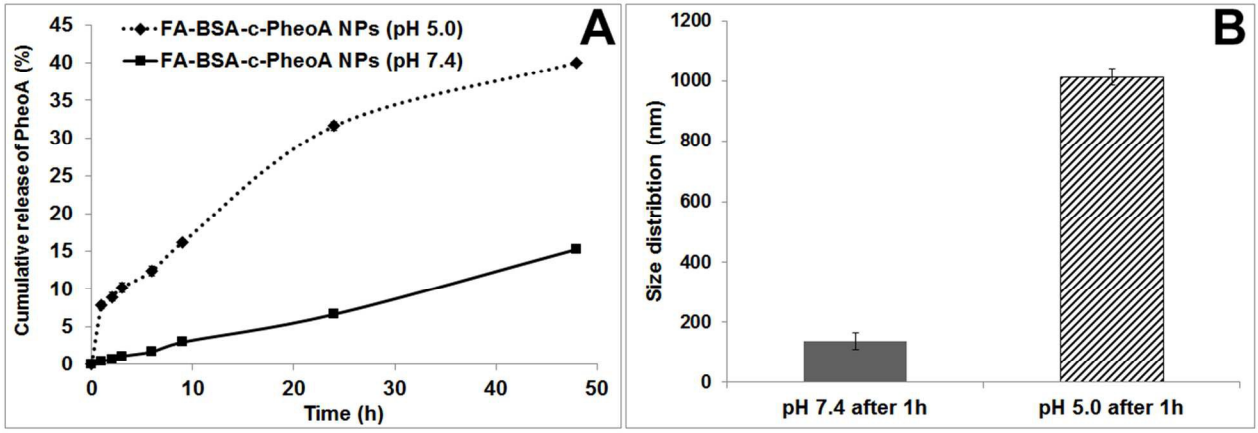

Figure 9. Release profile of PheoA from FA-BSA-c-PheoA NPs at different pH conditions through pH-responsive cleavage (A). Effect of pH on the size of FA-BSA-c-PheoA NP after 1 h incubation (B).

3.3. *In vitro* cellular uptake

The cellular uptake of free PheoA and FA-BSA-c-PheoA at different time points was assessed in B16F10 and MCF-7 cells, which have been reported to have regular expression of folate receptors on their surfaces [30, 31], by using confocal laser scanning microscopy (CLSM) utilizing the inherent fluorescence of PheoA (excitation 405 nm; emission 600–680 nm) to evaluate whether the folate-targeted NPs are internalized by receptor-mediated endocytosis as compared to free PheoA. The endosomal and lysosomal organelles in the B16F10 or MCF-7 cells were

stained with LysoTracker Green DND-26.

As shown in **Figure 10-I**, similar fluorescence was revealed for FA-BSA-c-PheoA NPs and free PheoA in B16F10 cells after 1.5 h of incubation, which was higher in intensity than the fluorescence observed for free BSA-c-PheoA (data not shown). These patterns were also observed after 3 h of incubation. The two fluorescences (red and green) overlay and were converted to a yellow signal, implicating that the NP was internalized into endosomes and lysosomes by endocytosis.

Moreover, significantly lower intensity from the FA-BSA-c-PheoA NPs was observed in the cells pre-treated with FA for 30 min, indicating that the folate receptors were occupied by FA. As a result, the internalization pathway of the FA-BSA-c-PheoA NPs by folate receptor-mediated endocytosis was blocked. On the other hand, the significant accumulation of free PheoA in the cells may be due to its lipophilicity. Highly lipophilic small molecules have been known to interact well with the cell membrane and internalize through simple diffusion, but *in vivo* these compounds aggregate before reaching the target site. Furthermore, the intensity of the red fluorescence in the cells treated with the FA-BSA-c-PheoA NPs for 3 h was higher than that in the cells treated for 1.5 h, indicating that the fluorescence of the PS was recovered through cleavage of the pH-sensitive linkage.

In MCF7 cells (**Figure 10-II**), the trend for cellular internalization of FA-BSA-c-Pheo NPs was similar to that found in B16F10 cells. Moreover, here FA blocking of the folate receptor was high and accordingly less internalization of FA-BSA-c-Pheo NP was observed because of the expression of the folate receptor in MCF7 cells.

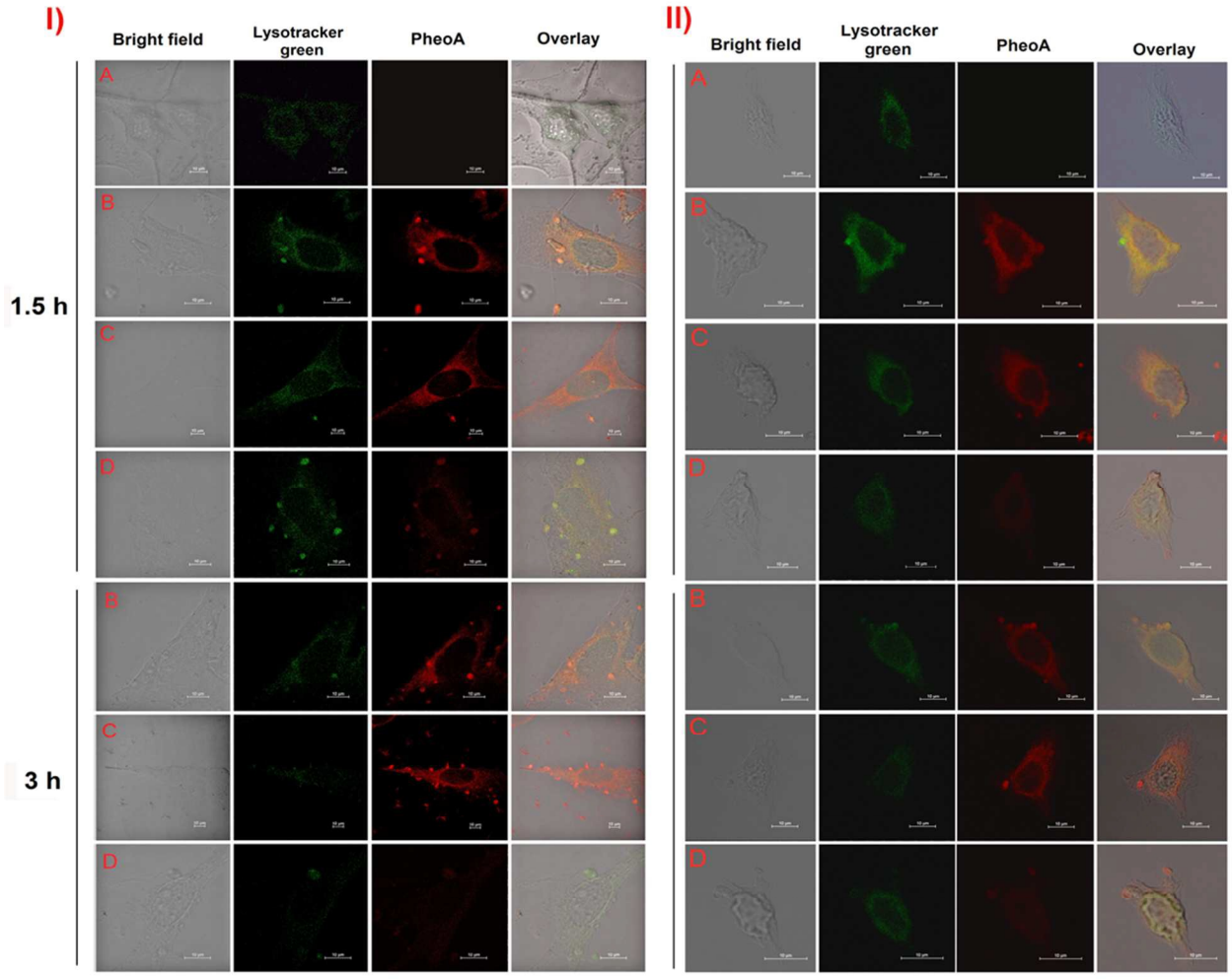

Figure 10. Confocal microscopic images of B16F10 cells **(I)** and MCF7 cells **(II)** treated with free pheophorbide-a (PheoA) and folate-bovine serum albumin-*cis*-PheoA nanoparticles at 1.5 and 3 h: (A) Control cells; (B) PheoA; (C) FA-BSA-c-PheoA NPs; and (D) FA + FA-BSA-c-PheoA NPs. In each image, the first column shows the images captured under differential interference contrast, the second column shows images captured under an Alexa 488 filter, the third column shows images captured under a Qdot655 filter, and the fourth column shows the overlay of images.

3.4. *In vitro* phototoxicity

In order to know the *in vitro* cytotoxicity of nanoparticle, we evaluated MTT assay on B16F10

and MCF7 cell lines with or without laser. As shown in **Figures 11A** and **C**, cells treated with 0.375 and 0.75 μg/mL of FA-BSA-c-PheoA NP for 6 h showed greater phototoxicity with did cells treated with BSA-c-PheoA. These results indicate that folate-receptor mediated cellular uptake of FA-BSA-c-PheoA may lead higher phototoxicity. In the other hand, phototoxicity of FA-BSA-c-PheoA NP at 0.75 μg/mL was slightly lower than that of free PheoA on MCF7 cell line, whereas at 1.5 μg/mL all showed high phototoxicity; the reason of high phototoxicity of free PheoA in DMSO may be that free PS is easily taken up by the cells through simple diffusion *in vitro* level. Overall, although phototoxicity of FA-BSA-c-PheoA NP and free PheoA is similar, FA-BSA-c-PheoA NP has advantage in *in vivo* level because of its biocompatibility and targeting property.

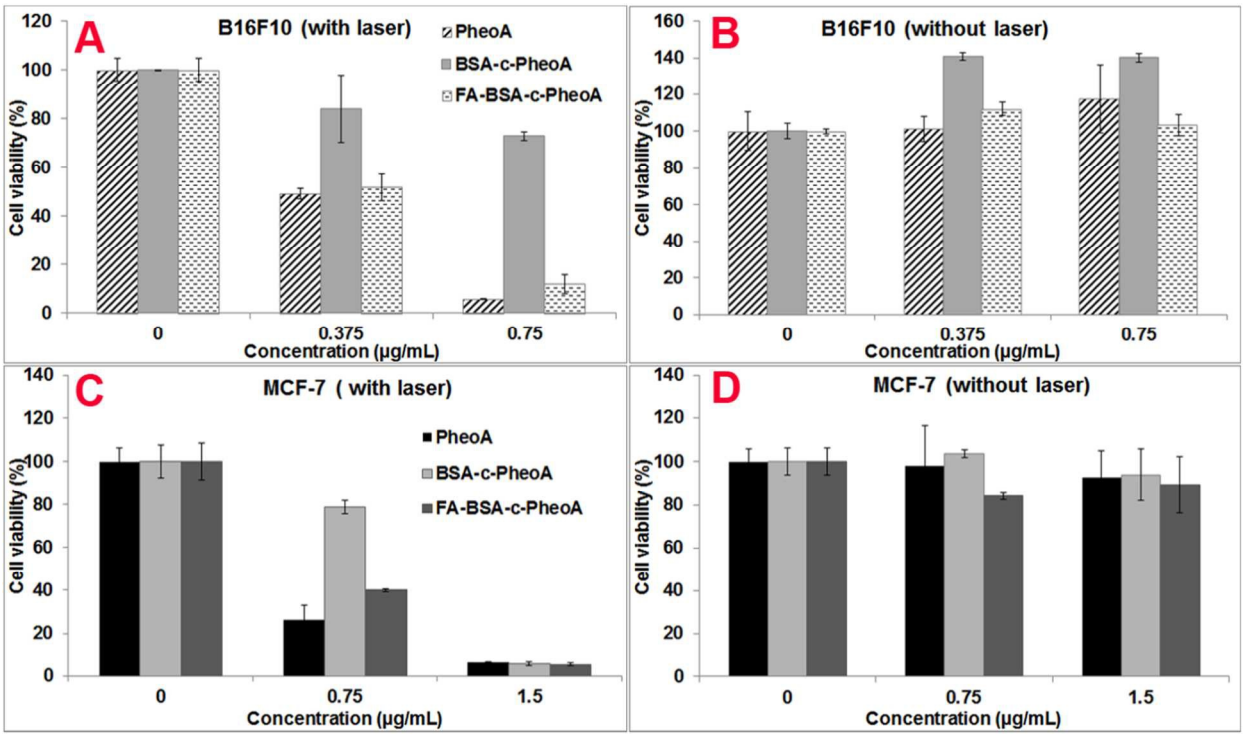

Figure 11. *In vitro* viability of cells exposed to the formulations indicated. B16F10 cells with (A) and without (B) laser; MCF-7 cells with (C) and without (D) laser, where PheoA in DMSO, BSA-c-PheoA and FA-BSA-c-PheoA nanoparticles in PBS. Cells were treated by laser for 20 min (1.5 J/cm^2) after 6 h incubation with formulations and further incubated for 24 h. The data represent the mean ± S.D. (n = 4).

There was not observed any dark toxicity from free PheoA and FA-BSA-c-PheoA NP against the both cells (**Figures 11B and D**).

3.5. *In vivo* biodistribution study

When the tumors reached 100 mm^3, the mice were administered with FA-BSA-c-PheoA NP or free PheoA (1 mg/kg of PheoA) via tail vein. As shown in **Figure 12-I**, fluorescence signal was observed in the tumor area of the FA-BSA-c-PheoA NP treated mice at 6 h and 24 h post-injection, whereas no fluorescence signal was revealed in the tumor area of the FA-BSA-c-

PheoA NP treated mice at 1 h post-injection, indicating that release and dequenching of PS from of the FA-BSA-c-PheoA NP get start after 1 h post-injection. As a comparison, free PheoA group showed high signal throughout the body, especially in the skin even at 1 h post-injection. At 24 h after injection, the organs of FA-BSA-c-PheoA NP treated mice were harvested for ex vivo imaging to study the biodistribution (**Figure 12-II**). The results showed that FA-BSA-c-PheoA NP preferentially accumulated at the tumor sites, likely due to the strong targeting effect through folate receptor on tumor cells.

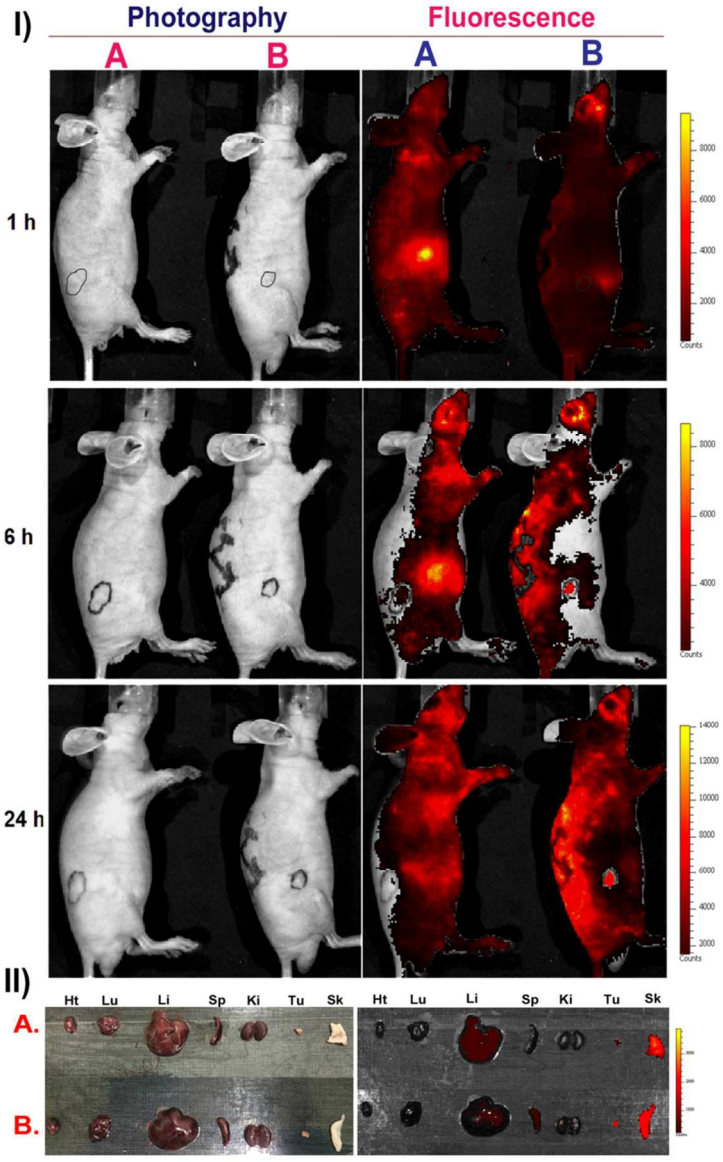

Figure 12. (**I**) *In vivo* distributions of PheoA (A) and FA-BSA-c-PheoA NP (B) visualized by using a molecular imaging system 1, 6 and 24 h after intravenous administration (PheoA 1 mg/kg). (**II**) *Ex vivo* near-infrared (NIR) fluorescence images and photography of tumor and major organs collected at 24 h after PheoA (A) and FA-BSA-c-PheoA NP (B) injection. Ht (heart), Lu (lung), Li (liver), Sp (spleen), Ki (kidney), Tu (tumor) and Sk (skin).

4. Discussion

In this study, we used PheoA, a widely employed chlorin derivative PS for PDT. In order to prepare an active-targeted theranostic NP for PDT and photodiagnosis, PheoA was first conjugated to BSA using a pH-responsive *cis*-aconityl linkage and the BSA-c-PheoA conjugate was then grafted with PEGylated FA. We hypothesized that covalently linking PheoA with albumin would increase the circulation half-life under physiological conditions and introducing an acid cleavable linkage between PheoA and BSA would allow PheoA to be released at a more specific site, for example, in the intracellular environment. In addition, by attaching folate to the NP, the selectivity of the PS for the target site, e.g., a tumor, would be improved, thereby increasing the possibility of site-specific accumulation and reducing the side effects related to poor selectivity.

Many studies have reported that folate conjugation has improved the targeting fate of therapeutic and imaging agents to tumors. For example, Syu et al. reported that folate-conjugated micelles loaded with PS reduced skin phototoxicity and lowered the effective dosage of PS by a third [32].

In addition, the FA-BSA-c-PheoA NPs have a mean diameter of around 120 nm, which is a desirable size because nanomaterials in the 100 nm range are known to be promising for systemic drug delivery [33].

In fact, instead of simply loading or encapsulating the PS in a nanoformulation, direct conjugation to biomolecules offers some advantages, including reducing the side effects related to early drug release and limiting the use of extra organic solvents for preparation of the nanoformulation [6]. In particular, albumin can be used for conjugation as much as needed without

any toxicity concerns owing to it being a component of blood, and the number of PS molecules attached to the albumin molecule could be increased owing to several functional groups in the albumin molecule. In this conjugate, five molecules of PheoA were attached to a BSA molecule, which is optimal but can be increased further. However, if extra external molecules are introduced into the BSA molecule, the inherent structure of albumin might be affected.

Use of a stimuli-responsive linkage between a therapeutic agent and a macromolecule can improve the site-specific delivery of therapeutic or imaging agents. Here, we used a *cis*-aconityl linkage, which is a widely employed, low-cost, pH-sensitive linker [34].

Through the conjugation of a PS with a macromolecule, the fluorescence of the PS can be quenched owing to its proximity to the macromolecule; however, upon cleavage of the pH-responsive linkage, the fluorescence would be recovered. As shown in the confocal study, the red fluorescence of PheoA increased in a time-dependent manner, indicating the dequenching of the fluorescence. Oh et al. reported that glycol-chitosan photosensitizer conjugate with disulfide bond showed similar efficiency with its free PS against cancer cells [18], which corresponds to our results, and futher the glycol-chitosan-PS conjugate revealed great anti-tumor efficiency in tumor-bearing mice.

Upon the *in vivo* biodistribution study, free PheoA had the relatively shorter circulation time and less tumor accumulation, which was a specific pharmacokinetic feature of small dye molecules [35]; whereas FA-BSA-c-PheoA NPs had the highest tumor targeting efficiency and longer circulation time. In addition, the strong fluorescence signals from livers at 24 h post injection indicated that free PheoA accumulated in the reticuloendothelial system. In contrast, week signals from livers implied that FA-BSA-c-PheoA NPs are far away from nonspecific

accumulation in the reticuloendothelial system due to its nanosized structure. In the both cases, high fluorescence from skin at 24 h post injection indicated that there may be some skin phototoxicity, however, upon the time going, it would be eliminated.

These findings supported the design rationale of the nanoparticles, where selectively accumulation and prolonged retention of PS in the tumor tissues with higher concentrations can be achieved through active targeting by folate-receptor mediated endocytosis.

Although our PS-albumin NP shows the promising *in vitro* and *in vivo* results, the issue related to wavelength shorter than 700 nm of PS, i.e., poor tissue penetration, should be solved for the clinical applications. As a possible solution, FA-BSA-c-PheoA NP can be combined with an upconversion nanoparticle, which emits visible photons after excitation by the near infrared light with 980 nm wavelenth.[36] The visible photons produced can then activate the photosensitizers combined with upconversion nanoparticles via resonance energy transfer and generate reactive oxygen species (ROS), resulting in potential PDT against cancer.[36-38] In addition, the development of light delivery technology into the exact location of a disorder might be a way to allow the application of visible light absorbing PSs for clinical PDT.[39]

5. Conclusion

In this study, we synthesized a pH-responsive BSA-c-PheoA conjugate and prepared folate-targeted BSA-c-PheoA self-assembling NPs of approximately 121 nm in size with a negative surface charge. This carrier was shown to have a good pH-responsive PS release profile and effective receptor-mediated cellular uptake. Folate-targeted nanoparticles showed significantly higher phototoxicity in B16F10 and MCF-7 cells compared to simple BSA-c-PheoA NPs. This

nanoparticulate system can also be utilized as an imaging agent because it has a strong fluorescence emission at 675 nm. The in vivo imaging data showed that FA-BSA-c-PhoeA NPs revealed enhanced tumor accumulation, indicating the ability to use the formulation as a theranostic agent. Through preparing this system, we are able to solve two issues related to hydrophobic photosensitizer, PheoA: one is our nanoparticle could be injected in aqueous solution due to albumin; the other one is that PheoA can be specifically delivered to folate-expressing tumor owing to folate ligand on the surface of NP. In the further study, we could overcome the issue related to the visible wavelength of PS in FA-BSA-c-PheoA NP, at which the light poorly penetrates through tissue, by means mentioned in the discussion section.

Acknowledgements: This research was supported by the Basic Science Research Program (NRF 2014R1A1A2053373) and the Pioneer Research Center Program (NRF 2014M3C1A3054153) through the National Research Foundation of Korea (NRF) funded by the Ministry of Education, Science and Technology.

References

1. P. Agostinis, K. Berg, K. A. Cengel, T. H. Foster, A. W. Girotti, S. O. Gollnick, S. M. Hahn, M. R. Hamblin, A. Juzeniene, D. Kessel, M. Korbelik, J. Moan, P. Mroz, D. Nowis, J. Piette, B. C. Wilson and J. Golab, *CA: a cancer journal for clinicians*, 2011, **61**, 250-281.
2. C. J. Ho, G. Balasundaram, W. Driessen, R. McLaren, C. L. Wong, U. S. Dinish, A. B. Attia, V. Ntziachristos and M. Olivo, *Scientific reports*, 2014, **4**, 5342.
3. A. Chatterjee, D. J. Oh, K. M. Kim, K. S. Youk and K. H. Ahn, *Chemistry, an Asian journal*, 2008, **3**, 1962-1967.
4. Y. Namiki, T. Namiki, M. Date, K. Yanagihara, M. Yashiro and H. Takahashi, *Pharmacological research : the official journal of the Italian Pharmacological Society*, 2004, **50**, 65-76.
5. Z. Sezgin, N. Yuksel and T. Baykara, *European journal of pharmaceutics and biopharmaceutics : official journal of Arbeitsgemeinschaft fur Pharmazeutische Verfahrenstechnik e.V*, 2006, **64**,

261-268.
6. S. A. Sibani, P. A. McCarron, A. D. Woolfson and R. F. Donnelly, *Expert opinion on drug delivery*, 2008, **5**, 1241-1254.
7. H. Park and K. Na, *Biomaterials*, 2013, **34**, 6992-7000.
8. I. Brigger, C. Dubernet and P. Couvreur, *Advanced drug delivery reviews*, 2002, **54**, 631-651.
9. S. Biswas and V. P. Torchilin, *Advanced drug delivery reviews*, 2014, **66C**, 26-41.
10. M. E. Davis, Z. G. Chen and D. M. Shin, *Nature reviews. Drug discovery*, 2008, **7**, 771-782.
11. G. V. Patil, *Drug Dev Res*, 2003, **58**, 219-247.
12. F. Kratz, *Journal of controlled release : official journal of the Controlled Release Society*, 2008, **132**, 171-183.
13. F. Kratz and A. Warnecke, *Journal of controlled release : official journal of the Controlled Release Society*, 2012, **164**, 221-235.
14. N. P. Desai, V. Trieu, L. Y. Hwang, R. Wu, P. Soon-Shiong and W. J. Gradishar, *Anti-cancer drugs*, 2008, **19**, 899-909.
15. H. Jeong, M. Huh, S. J. Lee, H. Koo, I. C. Kwon, S. Y. Jeong and K. Kim, *Theranostics*, 2011, **1**, 230-239.
16. W. J. Gradishar, *Expert opinion on pharmacotherapy*, 2006, **7**, 1041-1053.
17. F. Kratz, *Journal of controlled release : official journal of the Controlled Release Society*, 2014, **190**, 331-336.
18. I. H. Oh, H. S. Min, L. Li, T. H. Tran, Y. K. Lee, I. C. Kwon, K. Choi, K. Kim and K. M. Huh, *Biomaterials*, 2013, **34**, 6454-6463.
19. H. Kim, Y. Kim, I. H. Kim, K. Kim and Y. Choi, *Theranostics*, 2013, **4**, 1-11.
20. C. S. Lee and K. Na, *Biomacromolecules*, 2014, **15**, 4228-4238.
21. K. K. Ng, J. F. Lovell, A. Vedadi, T. Hajian and G. Zheng, *ACS nano*, 2013, **7**, 3484-3490.
22. Y. Li, K. Xiao, W. Zhu, W. Deng and K. S. Lam, *Advanced drug delivery reviews*, 2014, **66**, 58-73.
23. G. Battogtokh, H. B. Liu, S. M. Bae, P. K. Chaturvedi, Y. W. Kim, I. W. Kim and W. S. Ahn, *J Porphyr Phthalocya*, 2012, **16**, 1024-1031.
24. W. L. Ye, J. B. Du, B. L. Zhang, R. Na, Y. F. Song, Q. B. Mei, M. G. Zhao and S. Y. Zhou, *PloS one*, 2014, **9**, e97358.
25. J. H. Kang, G. Battogtokh and Y. T. Ko, *AAPS PharmSciTech*, 2014, **15**, 1087-1092.
26. B. C. Bae and K. Na, *Biomaterials*, 2010, **31**, 6325-6335.
27. O. Taratula, C. Schumann, M. A. Naleway, A. J. Pang, K. J. Chon and O. Taratula, *Molecular pharmaceutics*, 2013, **10**, 3946-3958.
28. G. Battogtokh and Y. T. Ko, *Pharmaceutical research*, 2014, **31**, 3019-3030.

29. G. Battogtokh, H. B. Liu, S. M. Bae, P. K. Chaturvedi, Y. W. Kim, I. W. Kim and W. S. Ahn, *J Photochem Photobiol B*, 2012, **110**, 50-57.
30. D. Hu, Z. Sheng, S. Fang, Y. Wang, D. Gao, P. Zhang, P. Gong, Y. Ma and L. Cai, *Theranostics*, 2014, **4**, 142-153.
31. T. Kurosaki, T. Morishita, Y. Kodama, K. Sato, H. Nakagawa, N. Higuchi, T. Nakamura, T. Hamamoto, H. Sasaki and T. Kitahara, *Molecular pharmaceutics*, 2011, **8**, 913-919.
32. W. J. Syu, H. P. Yu, C. Y. Hsu, Y. C. Rajan, Y. H. Hsu, Y. C. Chang, W. Y. Hsieh, C. H. Wang and P. S. Lai, *Small*, 2012, **8**, 2060-2069.
33. L. Zhang, F. X. Gu, J. M. Chan, A. Z. Wang, R. S. Langer and O. C. Farokhzad, *Clinical pharmacology and therapeutics*, 2008, **83**, 761-769.
34. F. Q. Hu, Y. Y. Zhang, J. You, H. Yuan and Y. Z. Du, *Molecular pharmaceutics*, 2012, **9**, 2469-2478.
35. C. L. Zhang, C. Li, Y. L. Liu, J. P. Zhang, C. C. Bao, S. J. Liang, Q. Wang, Y. Yang, H. L. Fu, K. Wang and D. X. Cui, *Adv Funct Mater*, 2015, **25**, 1314-1325.
36. C. Wang, L. Cheng and Z. Liu, *Theranostics*, 2013, **3**, 317-330.
37. S. H. Voon, L. V. Kiew, H. B. Lee, S. H. Lim, M. I. Noordin, A. Kamkaew, K. Burgess and L. Y. Chung, *Small*, 2014, **10**, 4993-5013.
38. N. M. Idris, M. K. Gnanasammandhan, J. Zhang, P. C. Ho, R. Mahendran and Y. Zhang, *Nat Med*, 2012, **18**, 1580-1585.
39. B. C. Wilson and M. S. Patterson, *Phys Med Biol*, 2008, **53**, R61-R109.

Graphical abstract